Received: 6 April 2022 | Revised: 24 May 2022 | Accepted: 23 June 2022

DOI: 10.4218/etrij.2022-0136

ORIGINAL ARTICLE

ETRI Journal WILEY

Joint resource optimization for nonorthogonal multiple access-enhanced scalable video coding multicast in unmanned aerial vehicle-assisted radio-access networks

Ziyuan Tong[1] | Hang Shen[1] | Ning Shi[2] | Tianjing Wang[1] | Guangwei Bai[1]

[1]College of Computer Science and Technology, Nanjing Tech University, Nanjing, China

[2]Nanjing Trusted Blockchain and Algorithm Economics Institute, Nanjing, China

Correspondence
Hang Shen, College of Computer Science and Technology, Nanjing Tech University, Nanjing, China.
Email: hshen@njtech.edu.cn

Funding information
National Natural Science Foundation of China under Grants 61502230 and 61501224, the National Project Funding for Key R&D Programs under Grant 2018YFC0808500, the Natural Science Foundation of Jiangsu Province under Grant BK20201357, and the Six Talent Peaks Project in Jiangsu Province under Grant RJFW-020.

Abstract

A joint resource-optimization scheme is investigated for nonorthogonal multiple access (NOMA)-enhanced scalable video coding (SVC) multicast in unmanned aerial vehicle (UAV)-assisted radio-access networks (RANs). This scheme allows a ground base station and UAVs to simultaneously multicast successive video layers in SVC with successive interference cancellation in NOMA. A video quality-maximization problem is formulated as a mixed-integer nonlinear programming problem to determine the UAV deployment and association, RAN spectrum allocation for multicast groups, and UAV transmit power. The optimization problem is decoupled into the UAV deployment–association, spectrum-partition, and UAV transmit-power–control subproblems. A heuristic strategy is designed to determine the UAV deployment and association patterns. An upgraded knapsack algorithm is developed to solve spectrum partition, followed by fast UAV power fine-tuning to further boost the performance. The simulation results confirm that the proposed scheme improves the average peak signal-to-noise ratio, aggregate video-reception rate, and spectrum utilization over various baselines.

KEYWORDS

nonorthogonal multiple access (NOMA), scalable video coding (SVC), spectrum partition, transmit-power adjustment, unmanned aerial vehicle (UAV)

1 | INTRODUCTION

High-definition video services have become the main driver for the rapid deployment of fifth-generation (5G) radio-access networks (RANs) [1], but the surge in video traffic results in a shortage of network resources. Video multicast uses the broadcast characteristics of wireless media to improve the transmission efficiency. Multicast can use the same wireless spectrum resources to send data from one data source to multiple target end devices (EDs). However, the ED with the worst channel quality in a multicast group acts as a bottleneck of the multicast rate, so the reception rates of each ED in the group must be ensured to achieve the required video quality.

Wireless video multicast using scalable video coding (SVC) can alleviate the bottleneck caused by EDs experiencing poor channel conditions [2,3]. SVC

separates a video stream into one basic video layer (BL) and multiple enhancement video layers (ELs). The EDs can decode different video layers depending on the channel conditions and decoding capabilities. Because of its robust error resistance, the absence of ELs cannot affect the BL's decoding and playback. Even if the EL is lost, the ED can decode the BL to watch the full video, albeit at lower definition. In the conventional SVC multicast confined to orthogonal multiple access (OMA), each video layer is transmitted over different orthogonal channels with reduced spectrum-utilization efficiency. Non-orthogonal multiple access (NOMA) can serve multiple EDs on the same channel through multiplexing in the power domain [4]. A transmitter can allocate different powers to each video layer, where the signal power arriving at each receiver is different. The receivers demodulate signals via successive interference cancellations (SICs) [5]. In this case, the video quality and resource efficiency achieved by NOMA outperform those by OMA, especially under diverse channel conditions [6].

The unmanned aerial vehicle (UAV)-assisted RAN architecture has excellent potential to enhance the quality and flexibility of SVC video multicasting. First, video multicast inherently suffers from the low resource utilization and video quality for EDs at the BS's coverage edge. For example, in large events, such as major sports events or concerts, off-site audiences and users with limited viewing angles usually watch live online. BSs in these areas inevitably become overloaded. In this case, UAVs can be temporarily deployed as air support to improve video services. Second, because they are more likely to establish line-of-sight (LoS) communication links, UAVs help reduce resource consumption during video transmission [7]. Third, UAVs can adjust their positions to enhance video reception in hotspot areas [8] and improve resource utilization by adjusting transmit power.

The above considerations motivate the development of a UAV-assisted SVC multicast scheme for NOMA-enabled cellular networks. However, SVC video multicast support in NOMA-enhanced networks faces significant challenges in determining the UAV deployment and transmit power, association patterns between UAVs and multicast groups, and resource allocation among multicast groups. First, the optimal multicast group association largely depends on UAV placement and resource allocation. Second, the UAV's transmit power significantly influences the sequential superposition of video layers and resource division among different multicast groups [9]. Third, owing to the unique channel model [10], each UAV has an effective coverage area determined by its altitude. Therefore, resource allocation must consider both the UAV locations and effective coverage.

1.1 | Related works

Most previous works studied resource management for SVC multicast in terrestrial networks, for which the optimization of power allocation is a research hotspot. Zhu and others explored multigroup resource allocation and intragroup power allocation [3]. Wu and others investigated the NOMA downlink relay transmission adapting vertical decomposition, and a layered power-allocation algorithm was proposed to maximize the throughput [11]. Liu and others proposed cooperative NOMA broadcasting/multicasting for vehicle-to-everything system to improve service and fairness. The formulated problem is transformed into a sequence of convex feasibility problems and solved by a bisection-based power-allocation algorithm [12]. Ahn and others investigated a cross-layer collaboration between SVC and layered-division multiplexing to enhance the reliability gain in broadcast/broadband cooperation [13].

Another line of research focuses on user grouping. Zhou and others designed cell range expansion and almost-blank subframe schemes to address the joint optimization of resource allocation and user association for SVC multicast [14]. Araniti and others studied the simultaneous transmission of the same content within multiple cells and designed a dynamic area-formation algorithm to increase the aggregate data rate [15]. Jiang and others proposed a novel user-grouping strategy in a quality-driven scalable video-transmission framework with cross-layer support for multiuser NOMA [16]. By analyzing the reliability and quality gains achieved by a broadcast–unicast convergent platform, Ahn and others proposed an optimal broadcast content-selection strategy to maximize transmission rates [17].

UAV-assisted resource provisioning has attracted academic attention, but little of the literature has considered integration with NOMA technology. By optimizing user scheduling and the UAV's trajectory, Pang and others present a UAV-assisted NOMA network to maximize the sum rate of UAV-served EDs [18]. A millimeter wave (mmWave)-enabled NOMA-UAV network was presented in Tang and others [19] to maximize energy efficiency by optimizing the UAV placement, hybrid precoding, and power allocation. Nguyen and others studied the iterative optimization of trajectory control and subchannel assignment for UAV-enabled wireless networks to maximize the minimum rate of EDs [20]. A joint height-optimization, channel-allocation, and power-allocation scheme for UAVs was developed to maximize the total rate of cell-edge EDs under UAV coverage [21]. Amin and others studied UAV-assisted backscatter networks, where a UAV acts as both a mobile power transmitter and an information collector. The tradeoff among UAV altitude,

number of backscatter devices, and backscatter coefficients was identified to maximize the number of decoded bits while minimizing UAV flight duration [22]. A UAV-aided NOMA scheme was explored in Wang and others [23] to achieve simultaneous wireless information and power transfer while guaranteeing secure transmission with passive ground receivers.

It remains open to debate whether UAV can boost NOMA-enabled SVC multicast, and it is necessary to investigate adaptive resource management and transmit-power adjustment (TPA). This paper explores the joint optimization for NOMA-enhanced SVC multicast in UAV-assisted RANs and identifies key factors that influence video quality.

1.2 | Contributions and organization

Considering BS–UAV cooperation, we study a resource-management problem for SVC multicast in NOMA-enhanced RANs to maximize the overall video quality at EDs in multicast groups. The main contributions are as follows:

1. A NOMA-enabled SVC video multicast scheme is proposed where a BS and UAVs transmit different video-layer signals in the power domain on the same channel. The joint optimization of UAV deployment, association pattern, spectrum division, and UAV TPA is formulated as a mixed-integer nonlinear programming (MINLP) problem considering video traffic statistics and environmental factors.
2. The proposed optimization problem is decoupled into UAV deployment-association (UDA), spectrum-partition (SP), and UAV TPA subproblems. A k-means-based heuristic method is adopted to determine the UAV deployment and association patterns for the UDA subproblem. An upgraded multiple-choice knapsack is then designed for the SP subproblem to determine the number of subchannels for each multicast group, along with fast power fine-tuning for the TPA subproblem to boost performance further.
3. Simulations demonstrate that the proposed scheme outperforms various baseline methods by significantly reducing complexity with little sacrifice in performance. The average peak signal-to-noise ratio (PSNR) of our method is at most 0.7% lower than that of the optimal solution and is equal in most cases.

The rest of the paper is organized as follows. In Section 2, we introduce the network model. Then, the joint optimization and solution are proposed in Sections 3 and 4, respectively. In Section 5, extensive simulation results are provided to evaluate the performance of our proposed protocol and algorithm. Finally, we conclude our paper in Section 6. The main symbols are listed in Table 1.

TABLE 1 Important symbols

Symbols	Definition
$a_{j,n}$	Association indicator for group n to UAV j
b_n	Number of subchannels allocated to the nth group
B	Total number of subchannels
$e_{j,s}$	Indicator for transmit power s selected by UAV j
$g_{m,i}$	Channel gain from the BS to ED i
$g_{j,i}$	Channel gain from UAV j to ED i
$h_{m,i}$	Horizontal distance between the BS and ED i
$h_{i,j}$	Horizontal distance between ED i and UAV j
$\mathcal{I}_n/I_n$	Set/number of EDs in multicast group n
$\mathcal{I}_{j,n}/I_{j,n}$	Set/number of EDs in $\mathcal{I}_n$ covered by UAV j
$\mathcal{J}/J$	Set/number of UAV IDs
$\mathcal{N}/N$	Set/number of multicast groups
$p_{j,s}$	Transmit power s selected by UAV j
p_m	Transmit power of the BS
$\mathrm{PSNR}_{1,n}$	PSNR of the BL received by group n
$\mathrm{PSNR}_{2,n}$	PSNR of the EL and the EL received by group n
R_j	Effective coverage radius of UAV j
$\mathcal{S}_j/S_j$	Set/number of transmit-power indexes for UAV j
$u_{1,n,i}/u_{2,n,i}$	BL/EL reception indicator for ED $i \in \mathcal{I}_n$
v_j	UAV deployment position (x_j, y_j, z_j)
w	Bandwidth of each subchannel
$z^{(\min)}/z^{(\max)}$	Lower/upper bound of UAV altitude
$\lambda_{l,n}$	Bit rate of the lth video layer requested by group n
$\eta_{\mathrm{LoS}}/\eta_{\mathrm{NLoS}}$	Additional path loss of the U2E link for LoS/NLoS
ξ	LoS probability threshold
ψ	Free-space path-loss threshold

2 | SYSTEM MODEL

Consider a UAV-assisted RAN, where multiple UAVs are placed within the communication coverage of a BS, as shown in Figure 1. It is assumed that UAVs have high-

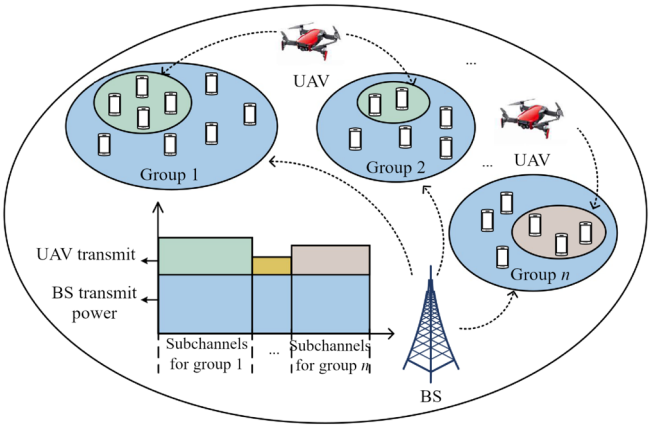

FIGURE 1 Unmanned aerial vehicle (UAV)-assisted scalable video coding (SVC) video multicast for multiple groups

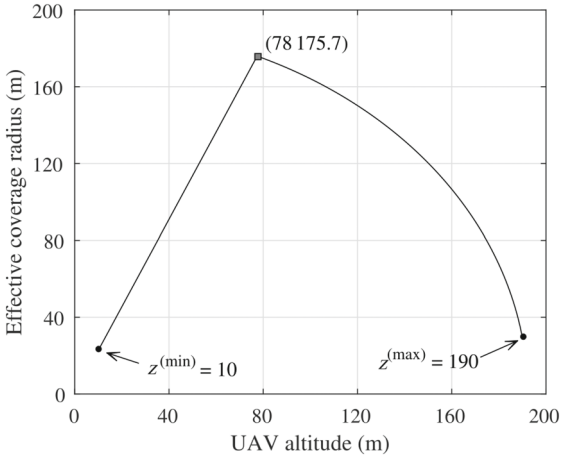

FIGURE 2 Effective unmanned aerial vehicle (UAV) coverage radius

capacity fronthaul links through free-space optics or mmWave to communicate with the BS to obtain video content [24]. When necessary, UAVs can harvest power from the BS via wireless power transfer [25]. All EDs are distributed randomly within the BS coverage. EDs requesting the same video stream belong to one multicast group.

2.1 | Layered video streams

SVC separates video streams into multiple video layers consisting of a BL and multiple ELs with different quality-level resolutions. In the system, the BS sends the BL to all the EDs, whereas UAVs send one EL to the EDs located at hot spots. The BL (EL) is referred to as the first (second) video layer. $\lambda_{l,n}$ is the bit rate of the lth video layer requested by multicast group n, which represents the minimum rate for normal video decoding. The video reception should reach the minimum rate at which the video can be played. Multiple video layers can be reconstructed into a complete video. The EL can be decoded if and only if the BL is completely received.

2.2 | UAV coverage model

There exist two types of communication links in video delivery: BS-to-ED link (B2E) and UAV-to-ED (U2E). Unlike the B2E channel, the U2E channel quality is influenced by factors such as UAV flight altitude, elevation angle, and probabilities of LoS or non-line-of-sight (NLoS) communications. The location coordinates of ED i are denoted as $(x_i, y_i, 0)$. Let $v_j = (x_j, y_j, z_j)$ represent the deployment position of UAV j. The LoS probability between UAV j and ED i is defined as [26]

$$P_{\mathrm{LoS}}(h_{i,j}, z_j) = \frac{1}{1 + o_1 \exp\left(-o_2\left(\arctan\left(\frac{z_j}{h_{i,j}}\right) - o_1\right)\right)}, \quad (1)$$

where $h_{i,j} = \sqrt{(x_i - x_j)^2 + (y_i - y_j)^2}$ represents the horizontal distance between ED i and UAV j. o_1 and o_2 are constants determined by environmental factors. The average path loss is given by [26]

$$\begin{aligned}\phi(h_{i,j}, z_j) = \; & 20 \log_{10}\left(\frac{4\pi c_1 \sqrt{h_{i,j}^2 + z_j^2}}{c_2}\right) + P_{\mathrm{LoS}}(h_{i,j}, z_j)\eta_{\mathrm{LoS}} \\ & + \left(1 - P_{\mathrm{LoS}}(h_{i,j}, z_j)\right)\eta_{\mathrm{NLoS}},\end{aligned} \quad (2)$$

where c_1 is the carrier frequency and c_2 is the speed of light. η_{LoS} and η_{NloS} represent the additional path loss of the U2E link for LoS and NLoS, respectively. The channel gain from UAV j to ED i is calculated as $g_{j,i} = 10^{-\phi(h_{i,j}, z_j)/10}$. The effective coverage radius of UAV j depends mainly on the LoS probability and free-space path loss, determined as [7,27]

$$R_j = \min\left\{\frac{z_j}{\tan\left(o_1 - \frac{1}{o_2}\ln\frac{1-\xi}{o_1\xi}\right)}, \sqrt{\left(\frac{c_2 10^{\frac{\psi}{20}}}{4\pi c_1}\right)^2 - z_j^2}\right\}, \quad (3)$$

where ξ represents the LoS probability for each UAV and ψ represents the threshold of free-space path loss. Figure 2 shows the impact of z_j on R_j in this scenario with $\xi = 89$ dB, $\psi = 0.5$, $o_1 = 9.61$, and $o_2 = 0.16$. The UAV's altitude ranges from the lower bound of $z^{(\min)} = 10$m to the upper bound of $z^{(\max)} = 190$m. Note that there is no simple linear relationship between z_j and R_j.

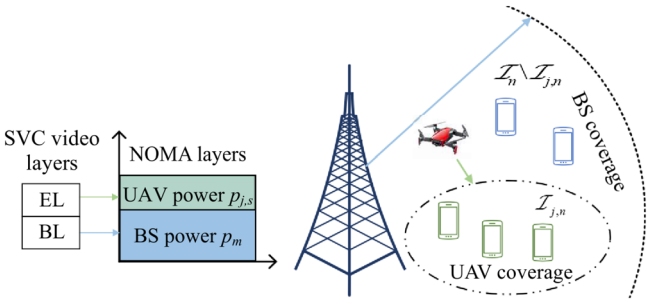

FIGURE 3 BS-unmanned aerial vehicle (UAV) cooperative multicast in nonorthogonal multiple access (NOMA)

R_j increases monotonically at first and then decreases with increasing z_j. When a UAV is flying at a height of 78 m, the effective coverage radius reaches its maximum of 175.7 m.

2.3 | UAV-assisted NOMA video multicast

Assume that B orthogonal subchannels can be allocated to N multicast groups, and the bandwidth of each subchannel is w. The number of subchannels allocated to multicast group n is denoted as b_n. Each multicast group is allocated different orthogonal subchannels and associated with at most one UAV, as shown in Figure 1. If transmit power s (denoted by $p_{j,s}$) is chosen by UAV j, the indication variable $e_{j,s}$ is set to 1; otherwise, it is set to 0. If multicast group n is associated with UAV j, indication variable $a_{j,n}$ is set to 1; otherwise, set to 0. The transmit power of the BS is denoted as p_m. Figure 3 provides an example to explain the cooperation between the BS and UAV j for multicast group n. The BS propagates the BL through the first NOMA layer using transmit power p_m, whereas UAV j transmits the EL via the second NOMA layer using transmit power $p_{j,s}$. These signals can be superimposed and coded in the power domain. Let $\mathcal{S}_j$ with set cardinality S_j denote the index set of optional transmit power for UAV j. Denote $\mathcal{J}$ as the ID set of available UAVs. The transmit power for subchannels allocated to multicast group n is

$$p_m + \sum_{j \in \mathcal{J}} \sum_{s \in \mathcal{S}_j} a_{j,n} e_{j,s} p_{j,s}.$$

The receivers at the EDs can conduct SIC decoding.

Let (x_m, y_m, z_m) denote the location coordinates of the BS. The set of EDs in multicast group n and its set cardinality are denoted as $\mathcal{I}_n$ and I_n, respectively. When multicast group n receives signals from the BL, the B2E channel gain from the BS to the ED $i \in \mathcal{I}_n$ is calculated as $g_{m,i} = 10^{-\left(\sqrt{h_{m,i}^2 + z_m^2}\right)^{\gamma}/10}$, where $h_{m,i} = \sqrt{(x_i - x_m)^2 + (y_i - y_m)^2}$ represents the horizontal distance between the BS and ED i and γ is the path-loss exponent. Because the BL's signals from the BS receive interference from the EL from UAV j with $p_{j,s}$, the achievable rate of decoding the BL's signals at ED $i \in \mathcal{I}_n$ is expressed as a function of $\mathcal{A}_n = \bigcup_{j \in \mathcal{J}} a_{j,n}$, b_n and $\mathcal{E} = \bigcup_{j \in \mathcal{J}, s \in \mathcal{S}_j} e_{j,s}$.

$$r_{m,n,i}(\mathcal{A}_n, b_n, \mathcal{E}) = b_n w \log_2 \left(1 + \frac{p_m g_{m,i}}{\sum_{j \in \mathcal{J}} \sum_{s \in \mathcal{S}_j} a_{j,n} e_{j,s} p_{j,s} g_{j,i} + \sigma^2}\right), \quad (4)$$

where σ^2 is the average background noise power. The constraint of ED $i \in \mathcal{I}_n$ to successfully receive/decode the BL can be expressed as

$$r_{m,n,i}(\mathcal{A}_n, b_n, \mathcal{E}) \geq \lambda_{1,n}. \quad (5)$$

Let $\mathcal{I}_{j,n}$ be the set of EDs in $\mathcal{I}_n$ covered by UAV j. The ID of the ED in $\mathcal{I}_{j,n}$ with maximum channel gain is expressed as

$$i_{j,n}^* = \arg \max_{i \in \mathcal{I}_{j,n}} g_{j,i}. \quad (6)$$

As the constraint of SIC and video-layer reconstruction, the signal strength of the BL received by ED $i_{j,n}^*$ must be greater than that of the EL, and the decision variable $e_{j,s}$ must satisfy

$$\sum_{s \in \mathcal{S}_j} e_{j,s} p_{j,s} g_{j,i_{j,n}^*} < \tau p_m g_{m,i_{j,n}^*}, \quad (7)$$

where $\tau \in (0,1)$ is a parameter to adapt to the environment. It can also be expressed as

$$\sum_{s \in \mathcal{S}_j} e_{j,s} p_{j,s} - \tau p_m \frac{g_{m,i_{j,n}^*}}{g_{j,i_{j,n}^*}} \leq 0. \quad (8)$$

ED $i \in \mathcal{I}_{j,n}$ can receive the EL's signal. Because there is no NOMA layer superimposed on the EL, the EL signal from UAV j with $p_{j,s}$ has no interference. The achievable rate of decoding the EL's signals at ED $i \in \mathcal{I}_{j,n}$ is expressed as a function of $\mathcal{A}_n$, b_n, and $\mathcal{E}$:

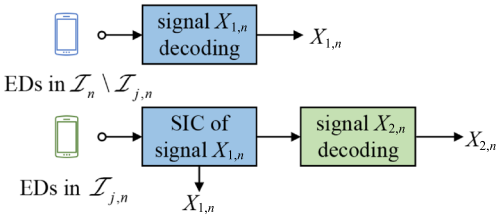

FIGURE 4 Interference cancellation in nonorthogonal multiple access (NOMA)

$$r_{j,n,i}(\mathcal{A}_n, b_n, \mathcal{E}) = b_n w \log_2\left(1 + \frac{\sum_{j \in \mathcal{J}} \sum_{s \in \mathcal{S}_j} a_{j,n} e_{j,s} p_{j,s} g_{j,i}}{\sigma^2}\right). \tag{9}$$

If both (5) and (10) are satisfied, the EL required by ED $i \in \mathcal{I}_{j,n}$ can be received/decoded successfully.

$$r_{j,n,i}(\mathcal{A}_n, b_n, \mathcal{E}) \geq \lambda_{2,n} \tag{10}$$

Figure 4 illustrates an example of SIC decoding. The BL is propagated through signal $X_{1,n}$ with the BS's transmit power, and the EL is propagated through signal $X_{2,n}$ with the UAV's transmit power. $X_{1,n}$ and $X_{2,n}$ are sent simultaneously. EDs in $\mathcal{I}_{j,n}$ can decode $X_{1,n}$ and $X_{2,n}$ with the BL and EL. EDs in $\mathcal{I}_n \setminus \mathcal{I}_{j,n}$ can decode $X_{1,n}$ with the BL without SIC.

3 | PROBLEM FORMULATION

In the proposed UAV-assisted SVC video-multicast framework, a challenging issue is determining how to deploy UAVs, selecting their transmit power and association patterns, and determining how many subchannels should be allocated to each multicast group.

Let $u_{1,n,i}$ be 1 if (5) is met and 0 otherwise. Let $u_{2,n,i}$ be 1 if both $u_{1,n,i} = 1$ and (10) are satisfied and 0 otherwise. The number of EDs that receive both the BL and EL in $\mathcal{I}_n$ is calculated by $\sum_{i \in \mathcal{I}_n} u_{2,n,i}$, and the number of EDs that only receive the BL in $\mathcal{I}_n$ is $\sum_{i \in \mathcal{I}_n} u_{1,n,i} - \sum_{i \in \mathcal{I}_n} u_{2,n,i}$. We use $\mathrm{PSNR}_{1,n}$ to denote the PSNR of the BL received by multicast group n and $\mathrm{PSNR}_{2,n}$ to represent the PSNR when both the BL and EL can be obtained. The PSNR of the video layers received by multicast group n with b_n subchannels is the sum of the two parts multiplied by $\mathrm{PSNR}_{2,n}$ and $\mathrm{PSNR}_{1,n}$. This can be expressed as a function of $\mathcal{V} = \bigcup_{j \in \mathcal{J}} v_j$, $\mathcal{A}_n$, b_n, and $\mathcal{E}$:

$$f_n(\mathcal{V}, \mathcal{A}_n, b_n, \mathcal{E}) = \sum_{i \in \mathcal{I}_n} u_{2,n,i} \mathrm{PSNR}_{2,n} + \left(\sum_{i \in \mathcal{I}_n} u_{1,n,i} - \sum_{i \in \mathcal{I}_n} u_{2,n,i}\right) \mathrm{PSNR}_{1,n}. \tag{11}$$

The set of multicast groups and its set cardinality are denoted as $\mathcal{N}$ and N, respectively. Based on (11), the aggregate PSNR for all multicast groups is expressed as a function of $\mathcal{V}$, $\mathcal{A} = \bigcup_{n \in \mathcal{N}} \mathcal{A}_n$, $\mathcal{B} = \bigcup_{n \in \mathcal{N}} b_n$, and $\mathcal{E}$.

$$f(\mathcal{V}, \mathcal{A}, \mathcal{B}, \mathcal{E}) = \sum_{n \in \mathcal{N}} f_n(\mathcal{V}, \mathcal{A}_n, b_n, \mathcal{E}). \tag{12}$$

The corresponding aggregate video-receiving rate of all EDs is calculated as

$$\sum_{l \in \{1,2\}} \sum_{n \in \mathcal{N}} \sum_{i \in \mathcal{I}_n} u_{l,n,i} \lambda_{l,n}.$$

The joint optimization of UAV deployment, association patterns, SP, and UAV transmit-power control to maximize (12) is formulated below.

$$\mathcal{P}1: \max_{\mathcal{V}, \mathcal{A}, \mathcal{B}, \mathcal{E}} : f(\mathcal{V}, \mathcal{A}, \mathcal{B}, \mathcal{E})$$

$$\text{s.t.} \begin{cases} r_{m,n,i}(\mathcal{A}_n, b_n, \mathcal{E}) - \varsigma u_{1,n,i} < \lambda_{1,n}, \forall n, i & \text{(13a)} \\ r_{m,n,i}(\mathcal{A}_n, b_n, \mathcal{E}) + \varsigma(1 - u_{1,n,i}) \geq \lambda_{1,n}, \forall n, i & \text{(13b)} \\ r_{j,n,i}(\mathcal{A}_n, b_n, \mathcal{E}) - \vartheta u_{2,n,i} u_{1,n,i} < \lambda_{2,n}, \forall n, i & \text{(13c)} \\ r_{j,n,i}(\mathcal{A}_n, b_n, \mathcal{E}) + \vartheta(1 - u_{2,n,i}) u_{1,n,i} \geq \lambda_{2,n}, \forall n, i & \text{(13d)} \\ a_{j,n}\left(\sum_{s \in S_j} e_{j,s} p_{j,s} - \tau p_m \frac{g_{m,i^*_{j,n}}}{g_{j,i^*_{j,n}}}\right) \leq 0, \forall j, n & \text{(13e)} \\ \sum_{s \in S_j} e_{j,s} - 1 = 0, \forall j & \text{(13f)} \\ \sqrt{x_j^2 + y_j^2} \leq R_m, \forall j & \text{(13g)} \\ z^{(\min)} \leq z_j \leq z^{(\max)}, \forall j & \text{(13h)} \\ \sum_{n \in \mathcal{N}} b_n \leq B & \text{(13i)} \\ \sum_{j \in \mathcal{J}} a_{j,n} \leq 1, \forall n & \text{(13j)} \\ e_{j,s} \in \{0,1\}, \forall j, s & \text{(13k)} \\ u_{l,n,i} \in \{0,1\}, \forall l \in \{1,2\}, n, i & \text{(13l)} \\ a_{j,n} \in \{0,1\}, \forall j, n & \text{(13m)} \end{cases}$$

In (13a) and (13b), ς is a sufficiently large constant to guarantee

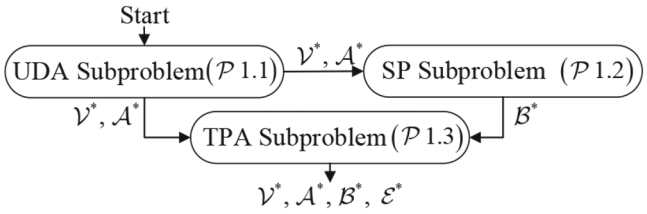

FIGURE 5 Problem-solving framework

$$u_{1,n,i}=\begin{cases}1, & r_{m,n,i}(\mathcal{A}_n,b_n,\mathcal{E})-\lambda_{1,n}>0\\ 0, & r_{m,n,i}(\mathcal{A}_n,b_n,\mathcal{E})-\lambda_{1,n}\le 0.\end{cases} \tag{14}$$

In (13c) and (13d), ϑ is a large enough constant to ensure

$$u_{2,n,i}=\begin{cases}1, & (r_{j,n,i}(\mathcal{A}_n,b_n,\mathcal{E})-\lambda_{2,n})u_{1,n,i}>0\\ 0, & (r_{j,n,i}(\mathcal{A}_n,b_n,\mathcal{E})-\lambda_{2,n})u_{1,n,i}\le 0.\end{cases} \tag{15}$$

Constraint (13e) is derived from (8). Constraint (13f) ensures that each UAV can only select one transmit power. Constraint (13g) states that each UAV's x–y-axis position must be within the BS's coverage radius, denoted as R_m. Constraint (13h) is the altitude scope, $[z^{(\min)}, z^{(\max)}]$, as in Figure 2, of each UAV. Constraint (13i) prevents the resource allocation across all multicast groups from exceeding the total number of subchannels. Under (13j), each multicast group can only associate with one UAV.

It is noted that ($\mathcal{P}1$) contains integer variables $e_{j,s}, b_n, a_{j,n}$ and continuous variable(s) $v_j(x_j,y_j,z_j)$. The nonlinear combinatorial transformation of the integer variables and the transformation of the continuous variables are conditioned by the objective and constraints. Thus, ($\mathcal{P}1$) belongs to a class of MINLP problems, which are generally NP-hard; thus, efficient algorithms must be designed to obtain a suboptimal solution.

4 | SOLUTIONS

($\mathcal{P}1$) is decomposed to the UDA, SP, and TPA subproblems to make it tractable and handleable. Problem solving consists of three sequential steps, as illustrated in Figure 5. (i) The UAV deployment positions, $\mathcal{V}^*$, and association patterns, $\mathcal{A}^*$, are obtained by the UDA subproblem. (ii) Given $\mathcal{V}^*$ and $\mathcal{A}^*$, the SP subproblem is solved to obtain the SP scheme, $\mathcal{B}^*$. (iii) Based on $\mathcal{A}^*, \mathcal{V}^*$, and $\mathcal{B}^*$, the optimal UAV transmit-power scheme, $\mathcal{E}^*$, is obtained by solving the TPA subproblem. We discuss the implementation details next.

4.1 | Solution to the UDA Subproblem

According to the UAV coverage model in Section 2.2, the number of EDs served by UAVs mainly depends on the altitude, given UAV deployment positions on the x–y plane. Therefore, we first determine the positions against hotspot areas on the x–y plane via k-means [28] and then adjust the UAVs' height.

The UDA subproblem aims to maximize the number of EDs under UAV coverage while optimizing their transmission performance by adjusting the UAVs' altitudes. Under the condition that the number of EDs served by UAV j (i.e., $\sum_{n\in\mathcal{N}} I_{j,n}$) remains unchanged, UAV j should reduce its altitude z_j to improve the transmission quality. For this purpose, the UAV altitude is determined as

$$z_j^*=\arg\min_{z_j\in[z^{(\min)},z^{(\max)}]}\left(\sum_{n\in\mathcal{N}} I_{j,n}+\frac{R_j}{\alpha}\right),\forall j\in\mathcal{J}, \tag{16}$$

where α is a constant that guarantees $R_j/\alpha\in(0,1)$. Combining (16), the UDA subproblem is formulated as ($\mathcal{P}1.1$).

$$\mathcal{P}1.1:\max_{\mathcal{V},\mathcal{A}}\sum_{j\in\mathcal{J}}\sum_{n\in\mathcal{N}} a_{j,n}I_{j,n}$$

$$\text{s.t. (13g) (13h) (13j) (16).} \tag{17}$$

The locations of all EDs and the number of UAVs are fed into k-means for clustering. The centroids in the output correspond to UAVs' deployment positions on the x–y plane, denoted by $\bigcup_{j\in\mathcal{J}}(x_j^*,y_j^*)$. By combining (x_j^*,y_j^*) with z_j^* in (16), UAV j is determined to be located at $v_j^*=(x_j^*,y_j^*,z_j^*)$, and the set of UAV deployment positions, $\mathcal{V}^*=\bigcup_{j\in\mathcal{J}} v_j^*$, is obtained. The ID of the UAV associated with multicast group n is expressed as

$$j_n^*=\arg\max_{j\in\mathcal{J}} I_{j,n}. \tag{18}$$

Based on (18), the association pattern between multicast group n and UAV j is

$$a_{j,n}^*=\begin{cases}1, & \text{if } j=j_n^*\\ 0, & \text{otherwise}\end{cases}, \tag{19}$$

which maximizes the number of EDs in the group (i.e., $\mathcal{I}_n$) under the coverage of UAV j. Then, the association scheme, $\mathcal{A}^*=\bigcup_{n\in\mathcal{N},j\in\mathcal{J}} a_{j,n}^*$, is obtained.

4.2 | Solution to the SP Subproblem

The spectrum partitioning relies on the UAV transmit power. Note that a UAV may be associated with multiple multicast groups. For each multicast group that associates with UAV j, the transmit power of the UAV needs to satisfy (13e). Thus, the transmit power of UAV j is initialized as

$$\hat{s}_j = \arg\min_{n \in \mathcal{N}} \left(\max_{s \in \mathcal{S}_j} a_{j,n} \left(p_{j,s} - \tau p_m \frac{g_{m,i^*_{j,n}}}{g_{j,i^*_{j,n}}} \right) \right). \tag{20}$$

The corresponding decision variable is determined by

$$\hat{e}_{j,s} = \begin{cases} 1, & \text{if } s = \hat{s}_j \\ 0, & \text{otherwise.} \end{cases} \tag{21}$$

By substituting $\mathcal{V}^*, \mathcal{A}^*$, and $\hat{\mathcal{E}} = \bigcup_{j \in \mathcal{J}, s \in \mathcal{S}} \hat{e}_{j,s}$ into ($\mathcal{P}$1), ($\mathcal{P}$1) is reformulated as ($\mathcal{P}$1.2) with reduced variables.

$$\mathcal{P}1.2: \max_{\mathcal{B}} : f(\mathcal{V}^*, \mathcal{A}^*, \mathcal{B}, \hat{\mathcal{E}})$$

$$\text{s.t.} (13a)\ (13b)\ (13c)\ (13d)\ (13i)\ (13l). \tag{22}$$

We now derive the upper bound of the number of subchannels allocated to multicast group n. Based on (4), (9), (18), and (21), in the case of $b_n = 1$, the minimum receiving rates for BL and EL at ED $i \in \mathcal{I}_n$ are calculated as

$$k_{1,n} = w \min_{i \in \mathcal{I}_n} \log_2 \left(1 + \frac{p_m g_{m,i}}{\sum_{j \in \mathcal{J}} \sum_{s \in \mathcal{S}_j} a^*_{j,n} \hat{e}_{j,s} p_{j,s} g_{j,i} + \sigma^2} \right) \tag{23}$$

and

$$k_{2,n} = w \min_{i \in \mathcal{I}_{j,n}} \log_2 \left(1 + \frac{\sum_{j \in \mathcal{J}} \sum_{s \in \mathcal{S}_j} a^*_{j,n} \hat{e}_{j,s} p_{j,s} g_{j,i}}{\sigma^2} \right). \tag{24}$$

According to (23) and (24), the upper bound of the number of subchannels allocated to multicast group n for a video layer is approximated as

$$b_n^{(\max)} = \max \left\{ \left\lceil \frac{\lambda_{1,n}}{k_{1,n}} \right\rceil, \left\lceil \frac{\lambda_{2,n}}{k_{2,n}} \right\rceil \right\}. \tag{25}$$

For the remaining b subchannels, the maximum PSNR of the first n multicast groups is denoted as $F(n,b)$. If $b \geq b_n^{(\max)}$, we only consider allocating $[0, b_n^{(\max)}]$ subchannels to multicast group n.

Based on recursion for (26), Algorithm 1 is designed to find the optimal solution for SP. The algorithm belongs to an upgraded knapsack via dynamic programming. N multicast groups can be regarded as N types of items, where each type has B items. These items need to be placed in a knapsack with a capacity of B. The b_nth item in the nth class has a profit (determined by $f_n(\mathcal{V}^*, \mathcal{A}_n^*, b_n, \hat{\mathcal{E}})$) and a weight (i.e., b_n). Essentially, one item is selected from each type to maximize the total profit while the total weight does not exceed the capacity. $F(n,b)$ is computed recursively from $n=1$ and $b=1$, which relies on the maximum total PSNR of the first $n-1$ multicast group(s) and $f_n(\mathcal{V}^*, \mathcal{A}_n^*, b_n, \hat{\mathcal{E}})$. Inappropriate subchannel numbers are filtered based on (26) to reduce unnecessary calculations. After NB iterations, the optimal total PSNR ($F(N,B)$) and the spectrum-allocation scheme (i.e., $\mathcal{B}^* = \bigcup_{n \in \mathcal{N}} b_n^*$) can be obtained.

$$F(n,b) = \begin{cases} \max_{0 \leq b_n \leq b} F(n-1, b-b_n) + f_n\left(\mathcal{V}^*, \mathcal{A}_n^*, b_n, \hat{\mathcal{E}}\right), \text{if} b < b_n^{(\max)} \\ \max_{0 \leq b_n \leq b_n^{(\max)}} F(n-1, b-b_n) + f_n\left(\mathcal{V}^*, \mathcal{A}_n^*, b_n, \hat{\mathcal{E}}\right), \text{ if } b \geq b_n^{(\max)}. \end{cases} \tag{26}$$

Algorithm 1 Spectrum partition

Input: $\mathcal{V}^*$, $\mathcal{A}^*$, B, $\hat{\mathcal{E}}$
Output: $\mathcal{B}^*$

```
m ← 0;
for b ← 1 to B do
    F(0, b) ← 0;
end for
for n ← 1 to N do
    for b ← 1 to B do
        b*_n ← 0;
        F(n, b) ← F(n − 1, b);
        for b′ ← 1 to b do
            if b′ > b_n^(max) then
                break;
            end if
            m ← F(n − 1, b − b′) + f_n(V*, A*_n, b′, Ê);
            if F(n, b) < m then
                F(n, b) ← m; b*_n ← b′;
            end if
        end for
    end for
end for
return B* = ⋃_{n∈N} b*_n;
```

4.3 | Solution to the TPA Subproblem

Because the resource utilization is confined to the initialized UAV transmit power determined by (21), it is necessary to fine-tune the power to boost performance. Given $\mathcal{V}^*$, $\mathcal{A}^*$ and $\mathcal{B}^*$, the TPA subproblem is formulated as

$$\mathcal{P}1.3: \max_{\mathcal{E}}: f(\mathcal{V}^*\mathcal{A}^*,\mathcal{B}^*,\mathcal{E})$$

$$\text{s.t. (13a) (13b) (13c) (13d) (13e) (13f) (13k) (13l).} \quad (27)$$

Because there is no coupling among the decision variables in $\mathcal{E}$, ($\mathcal{P}$1.3) can be transformed to maximize the aggregate PSNR of the multicast groups associated with UAV j:

$$\sum_{n\in\mathcal{N}} a^*_{j,n} f_n(\mathcal{V}^*, \mathcal{A}^*_n, b^*_n, \mathcal{E}).$$

A fast search policy is developed in Algorithm 2 to optimize the transmit power of each UAV. Assume that all indexes are sorted in order of increasing UAV transmit power. The algorithm searches downwards starting from the initialized power (line 3), $\hat{s}_j$, to speed up the search. In other words, the strategic space of transmit power for UAV j is reduced to

$$\widehat{\mathcal{S}}_j = \{s \in \mathcal{S}_j | p_{j,s} \le p_{j,\hat{s}_j}\}. \quad (28)$$

Algorithm 2 Fast transmit-power fine-tuning

Input: $\mathcal{V}^*, \mathcal{A}^*, \mathcal{B}^*, \widehat{s}_j$
Output: $\mathcal{E}^*$
1: **for** $j' \leftarrow 1$ to J **do**
2: $t' \leftarrow 0$; $t \leftarrow 0$;
3: **for** $s' \leftarrow \widehat{s}_j$ to 1 **do**
4: Every element in $\mathcal{E}$ is set to 0;
5: $e_{j',s'} \leftarrow 1$;
6: $t \leftarrow \sum_{n\in\mathcal{N}} a^*_{j,n} f_n(\mathcal{V}^*, \mathcal{A}^*_n, b^*_n, \mathcal{E})$;
7: **if** $t > t'$ **then**
8: $t' \leftarrow t$; $\mathcal{E}^* \leftarrow \mathcal{E}$;
9: **end if**
10: **end for**
11: **end for**
12: **return** $\mathcal{E}^*$;

4.4 | Computational complexity analysis

In ($\mathcal{P}$1.1), the complexity of k-means is $O\left(\sum_{n\in\mathcal{N}} I_n\right)$, and association pattern calculations need to search for all $1 \le n \le N$ and $1 \le j \le J$, with a complexity of $O(NJ)$. For ($\mathcal{P}$1.2), the PSNR for multicast group n with b_n subchannels (determined by $f_n(\mathcal{V}^*, \mathcal{A}^*_n, b_n, \hat{\mathcal{E}})$) should be computed over all $1 \le n \le N$ and $1 \le b \le B$. Every iteration has a maximum complexity of $O(B)$. Thus, the worst-case complexity is $O(NB^2)$. Based on (28), the complexity of Algorithm 2 to solve ($\mathcal{P}$1.3) is $O\left(\sum_{j\in\mathcal{J}} \hat{S}_j\right)$, where $\hat{S}_j$ is the cardinality of $\hat{\mathcal{S}}_j$. The accumulative computational complexity reaches $O\left(\sum_{n\in\mathcal{N}} I_n + NJ + NB^2 + \sum_{j\in\mathcal{J}} \hat{S}_j\right)$, which is lower than complexity of ($\mathcal{P}$1). We later verify whether the proposed scheme can approach the optimal solution or directly achieve it.

5 | PERFORMANCE EVALUATION

5.1 | Experiment design

Extensive numerical simulations are conducted in MATLAB to verify the effectiveness and superiority of the proposed solution. A real video trace from Lee and others [29], consisting of 10 standard video test sequences with different video layers, along with the average bite rate and PSNR of each video layer, is utilized to make the simulations more realistic. The detailed parameters are listed in Table 2.

To evaluate the performance of the proposed strategy, we compare it with the optimal solution and the following four other baseline schemes:

TABLE 2 Parameter settings

Parameters	Values
Altitude of the BS (z_m)	10 m
Coverage radius of the BS (R_m)	800 m
BS transmit power (p_m)	10000 mW
Optional UAV transmit power ($p_{j,s}$)	{1, 2, ..., 8} mW
Scope of UAV altitude ($[z^{(\min)}, z^{(\max)}]$)	[10 m,190 m]
Parameters of UAV ($o_1/o_2/\eta_{\text{LoS}}/\eta_{\text{NLoS}}$)	9.61/0.16/1/20
Carrier frequency (c_1)	3.5 GHz [30]
LoS probability threshold (ξ)	0.5
Free-space path-loss threshold (ψ)	89 dB
Average background noise power (σ^2)	−174 dBm
Power parameter (τ)	0.8
Subchannel bandwidth (w)	180 kHz
Number of subchannels (B)	8–16
Number of multicast groups (N)	7
Number of EDs for multicast group n (I_n)	35

- **Optimal solution**, which relies on exhaustion to find the optimal solution to observe how the proposed method approaches the upper bound of performance.
- **OMA + Alg-1**, in which the BS and UAV multicast the BL and EL to a multicast group over orthogonal channels with fixed transmit power.
- **NOMA + Alg-1 + power fixed (PF)** [21], which focuses on optimizing the spectrum resource allocation without considering UAV transmit power.
- **NOMA + Resource Averaging (RA) + Alg-2**, which adjusts the UAV transmit power via Algorithm 2 and equally allocates subchannels among N multicast groups.

5.2 | Result analysis

5.2.1 | Impact of the number of available subchannels

Figure 6 shows the average PSNR for each ED as the number of subchannels varies from 8 to 16. Three subfigures are generated to observe the effect of the number of UAVs in more detail. With the increase in b_n that can support the transmission of more video layers, the average PSNR for each scheme increases, then tends to remain unchanged when B is large enough. First, the proposed plan consumes fewer spectrum resources than the OMA-based solution. Second, the proposed scheme can achieve a greater average PSNR than OMA + Alg-1, even with few spectrum resources. Because the proposed UAV transmit power-adaptation scheme mitigates the interference of EL signals with BL signals, our proposed method is improved by 0.5 dB over the NOMA + Alg-1 + PF when $J = 4$ and $B = 8$. Third, the proposed SP outperforms the RA strategy of NOMA + RA + Alg-2. Figure 7 shows the aggregate video-receiving rate with the same parameters as Figure 6. Compared with OMA + Alg-1, our scheme's aggregate video-receiving rate has increased by 15% when $J = 4$ and $B = 8$. The proposed scheme achieves the highest PSNR and aggregate video-receiving rate and approximates or directly obtains the optimal solution.

5.2.2 | Impact of the number of UAVs

Figure 8 depicts the average PSNR and aggregate video-receiving rate as the number of UAVs varies from 1 to 4

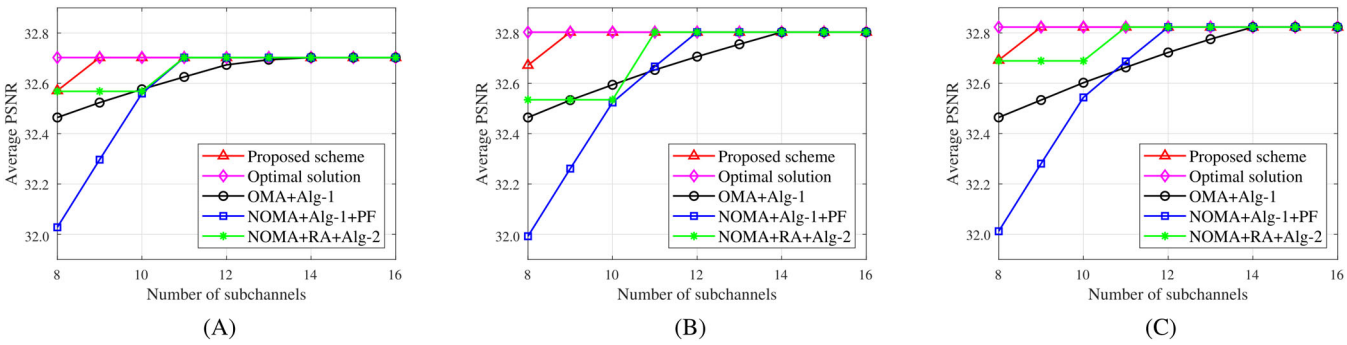

FIGURE 6 Average peak signal-to-noise ratio (PSNR) for each end device (ED) with varying subchannels: (A) 2 unmanned aerial vehicles (UAVs), (B) 3 UAVs, and (C) 4 UAVs

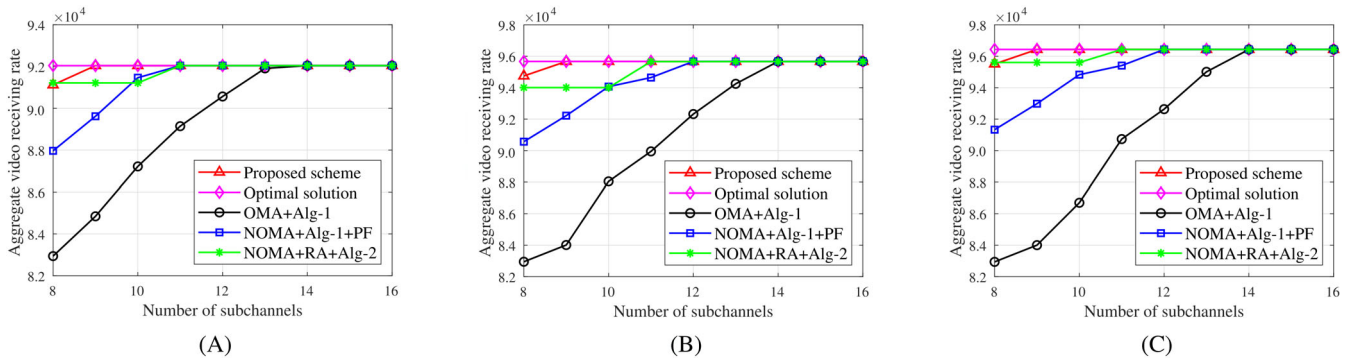

FIGURE 7 Aggregate video-receiving rate with varying subchannels: (A) 2 unmanned aerial vehicles (UAVs), (B) 3 UAVs, and (C) 4 UAVs

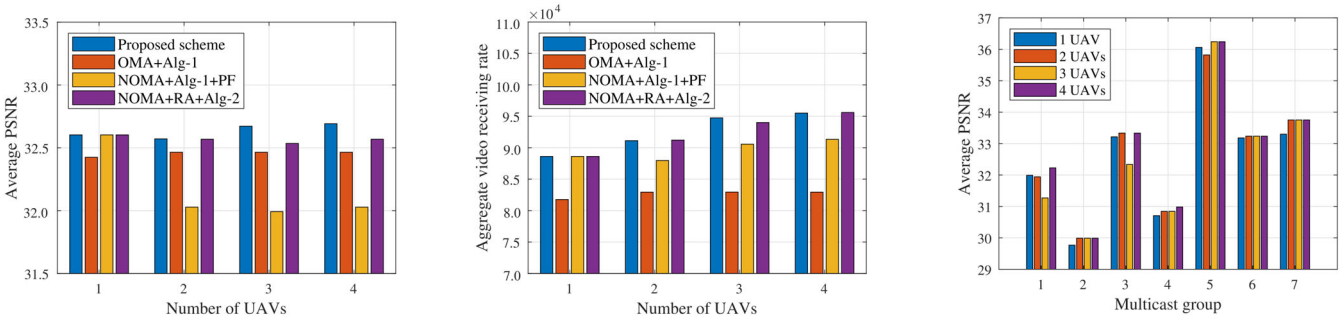

FIGURE 8 Average peak signal-to-noise ratio (PSNR) and aggregate video-receiving rate with varying number of unmanned aerial vehicles (UAVs): (A) Average PSNR for each end device (ED), (B) aggregate video-receiving rate, and (C) average PSNR for each multicast group

with B fixed to 8. The increase in the number of UAVs enables more EDs to be covered, which boosts the average PSNR and aggregate video-receiving rate. In OMA + Alg-1, the resources used to transmit the BL are insufficient. Even with more available UAVs, it is difficult to increase the average PSNR. The closer the EDs' hotspot is to the edge of the BS coverage, the worse the channel conditions. In NOMA + Alg-1 + PF, the UAVs' transmit power fails to adapt to heterogeneous channel conditions. Owing to the efficient resource utilization in NOMA and transmit-power adaptation, the proposed scheme is superior to the other three schemes. In particular, when resources are scarce, the video service in hotspot areas can be prioritized to boost overall performance. Differences in the number of UAVs lead to different UAV placements obtained via k-means clustering and association patterns. From Figure 8C, an increase in the number of UAVs improves the received video quality in most cases.

6 | CONCLUSION

We have presented a NOMA-enhanced SVC multicast scheme for UAV-assisted RANs. Resource management is studied to maximize the aggregate PSNR received by all the EDs. Because this joint optimization problem of UAV deployment, association patterns between UAVs and multicast groups, spectrum allocation, and UAV transmit-power selection is an MINLP problem, it is decoupled into three subproblems to facilitate its solution. Low-complexity heuristic algorithms are devised to determine UAV deployment, association patterns, spectrum allocation, and UAV transmit power. Simulation results with real-trace confirm that the proposed scheme improves significantly upon previous schemes over other benchmarks. In ongoing work, we plan to develop a dynamic cooperative deployment mechanism for UAVs to adapt to complex video-service scenarios.

CONFLICT OF INTEREST

The authors declare that there are no conflicts of interest.

ORCID

Hang Shen https://orcid.org/0000-0002-8804-2787

REFERENCES

1. I.-S. Comşa, G.-M. Muntean, and R. Trestian, *An innovative machine-learning-based scheduling solution for improving live UHD video streaming quality in highly dynamic network environments*, IEEE Trans. Broadcast. **67** (2021), no. 1, 212–224.
2. M. Ghermezcheshmeh, V. Shah-Mansouri, and M. Ghanbari, *Analysis and performance evaluation of scalable video coding over heterogeneous cellular networks*, Comput. Netw. **148** (2019), 151–163.
3. H. Zhu, Y. Cao, T. Jiang, and Q. Zhang, *Scalable NOMA multicast for SVC streams in cellular networks*, IEEE Trans. Commun. **66** (2018), no. 12, 6339–6352.
4. L. Dai, B. Wang, Y. Yuan, S. Han, I. Chih-lin, and Z. Wang, *Non-orthogonal multiple access for 5G: solutions, challenges, opportunities, and future research trends*, IEEE Commun. Mag. **53** (2015), no. 9, 74–81.
5. Z. Ding, Y. Liu, J. Choi, Q. Sun, M. Elkashlan, I. Chih-Lin, and H. V. Poor, *Application of non-orthogonal multiple access in LTE and 5G networks*, IEEE Commun. Mag. **55** (2017), no. 2, 185–191.
6. M. Zhang, H. Lu, F. Wu, and C. W. Chen, *NOMA-based scalable video multicast in mobile networks with statistical channels*, IEEE Trans. Mobile Comput. **20** (2021), no. 6, 2238–2253.
7. H. Shen, Q. Ye, W. Zhuang, W. Shi, G. Bai, and G. Yang, *Drone-small-cell-assisted resource slicing for 5G uplink radio access networks*, IEEE Trans. Veh. Technol. **70** (2021), no. 7, 7071–7086.
8. N. Zhao, F. R. Yu, L. Fan, Y. Chen, J. Tang, A. Nallanathan, and V. C. M. Leung, *Caching unmanned aerial vehicle-enabled small-cell networks: employing energy-efficient methods that store and retrieve popular content*, IEEE Veh. Technol. Mag. **14** (2019), no. 1, 71–79.

9. S. M. R. Islam, N. Avazov, O. A. Dobre, and K. Kwak, *Power-domain non-orthogonal multiple access (NOMA) in 5G systems: Potentials and challenges*, IEEE Commun. Surveys Tuts. **19** (2017), no. 2, 721–742.
10. A. A. Khuwaja, Y. Chen, N. Zhao, M.-S. Alouini, and P. Dobbins, *A survey of channel modeling for UAV communications*, IEEE Commun. Surveys Tuts. **20** (2018), no. 4, 2804–2821.
11. Y. Wu, L. P. Qian, H. Mao, X. Yang, H. Zhou, and X. Shen, *Optimal power allocation and scheduling for non-orthogonal multiple access relay-assisted networks*, IEEE Trans. Mobile Comput. **17** (2018), no. 11, 2591–2606.
12. G. Liu, Z. Wang, J. Hu, Z. Ding, and P. Fan, *Cooperative NOMA broadcasting/multicasting for low-latency and high-reliability 5G cellular V2X communications*, IEEE Internet Things J. **6** (2019), no. 5, 7828–7838.
13. S. Ahn, S.-I. Park, J.-Y. Lee, N. Hur, and J. Kang, *Cooperation between ldm-based terrestrial broadcast and broadband unicast: on scalable video streaming applications*, IEEE Trans. Broadcast. **67** (2021), no. 1, 2–22.
14. H. Zhou, Y. Ji, X. Wang, and B. Zhao, *Joint resource allocation and user association for SVC multicast over heterogeneous cellular networks*, IEEE Trans. Wireless Commun. **14** (2015), no. 7, 3673–3684.
15. G. Araniti, F. Rinaldi, P. Scopelliti, A. Molinaro, and A. Iera, *A dynamic MBSFN area formation algorithm for multicast service delivery in 5G NR networks*, IEEE Trans. Wireless Commun. **19** (2020), no. 2, 808–821.
16. X. Jiang, H. Lu, and C. W. Chen, *Enabling quality-driven scalable video transmission over multi-user NOMA system*, (IEEE INFOCOM - IEEE Conference on Computer Communications, Honolulu, HI, USA), Apr. 2018, pp. 1952–1960.
17. S. Ahn, S.-I. Park, J.-Y. Lee, N. Hur, Y. Wu, L. Zhang, W. Li, and J. Kim, *Large-scale network analysis on noma-aided broadcast/unicast joint transmission scenarios considering content popularity*, IEEE Trans. Broadcast. **66** (2020), no. 4, 770–785.
18. X. Pang, Z. Li, X. Chen, Y. Cao, N. Zhao, Y. Chen, and Z. Ding, *UAV-aided NOMA networks with optimization of trajectory and precoding*, (International Conference on Wireless Communications and Signal Processing, Hangzhou, China), Oct. 2018, pp. 1–6.
19. P. X, J. Tang, N. Zhao, Z. X, and Q. Y, *Energy-efficient design for mmwave-enabled noma-uav networks*, Sci. China Inf. Sci. **64** (2021), no. 4, 14.
20. M. D. Nguyen, L. Bao Le, and A. Girard, *Trajectory control and resource allocation for UAV-based networks with wireless backhauls*, (ICC-IEEE International Conference on Communications, Montreal, Canada), June 2021, pp. 1–6.
21. D. Zhai, H. Li, X. Tang, R. Zhang, Z. Ding, and F. R. Yu, *Height optimization and resource allocation for NOMA enhanced UAV-aided relay networks*, IEEE Trans. Commun. **69** (2021), no. 2, 962–975.
22. A. Farajzadeh, O. Ercetin, and H. Yanikomeroglu, *UAV data collection over noma backscatter networks: UAV altitude and trajectory optimization*, (ICC-IEEE International Conference on Communications, Shanghai, China), May 2019, pp. 1–7.
23. W. Wang, J. Tang, N. Zhao, X. Liu, X. Y. Zhang, Y. Chen, and Y. Qian, *Joint precoding optimization for secure SWIPT in UAV-aided NOMA networks*, IEEE Trans. Commun. **68** (2020), no. 8, 5028–5040.
24. M. S. Shokry, D. Ebrahimi, C. Assi, S. Sharafeddine, and A. Ghrayeb, *Leveraging UAVs for coverage in cell-free vehicular networks: a deep reinforcement learning approach*, IEEE Trans. Mobile Comput. **20** (2021), no. 9, 2835–2847.
25. X. Hu, K.-K. Wong, and Y. Zhang, *Wireless-powered edge computing with cooperative uav: task, time scheduling and trajectory design*, IEEE Trans. Wireless Commu. **19** (2020), no. 12, 8083–8098.
26. A. Al-Hourani, S. Kandeepan, and S. Lardner, *Optimal LAP altitude for maximum coverage*, IEEE Wireless Commun. Lett. **3** (2014), no. 6, 569–572.
27. W. Shi, J. Li, W. Xu, H. Zhou, N. Zhang, S. Zhang, and X. Shen, *Multiple drone-cell deployment analyses and optimization in drone assisted radio access networks*, IEEE Access **6** (2018), 12518–12529.
28. H. Qu, W. Zhang, J. Zhao, Z. Luan, and C. Chang, *Rapid deployment of UAVs based on bandwidth resources in emergency scenarios*, (Information Communication Technologies Conference, Nanjing, China), 2020, pp. 86–90.
29. J. Lee, B. C. Yeo, J.-S. Kim, M. S. Jang, and J. K. Choi, *Energy efficient scalable video coding based cooperative multicast scheme with selective layer forwarding*, IEEE Wireless Commun. Lett. **17** (2013), no. 6, 1116–1119.
30. I.-P. Belikaidis, A. Georgakopoulos, E. Kosmatos, V. Frascolla, and P. Demestichas, *Management of 3.5-GHz spectrum in 5G dense networks: a hierarchical radio resource management scheme*, IEEE Veh. Technol. Mag. **13** (2018), no. 2, 57–64.

AUTHOR BIOGRAPHIES

Ziyuan Tong received the BS degree in Computer Science from Nanjing University Jinling College, Nanjing, China. She is currently an MS student at the Department of Computer Science and Technology, Nanjing Tech University, Nanjing, China. Her research interests include space–air–ground integrated networks, nonorthogonal multiple access, resource management, and layer-aware wireless multicasting.

Hang Shen is currently an Associate Professor with the Department of Computer Science and Technology, Nanjing Tech University, Nanjing, China. He received the PhD degree (with honors) in Computer Science from the Nanjing University of Science and Technology. He worked as a Full-Time Postdoctoral Fellow with the Broadband Communications Research (BBCR) Lab, Department of Electrical and Computer Engineering, University of Waterloo,

Waterloo, ON, Canada, from 2018 to 2019. His research interests involve space–air–ground integrated networks, network security, and privacy computing. He serves as an Associate Editor for IEEE ACCESS, an Academic Editor for *Mathematical Problems in Engineering*, and served as a Guest Editor for *Peer-to-Peer Networking and Applications*.

Shi Ning holds a bachelor's degree from Tsinghua University and a doctorate from Hong Kong University of Science and Technology. He is a leading domestic researcher in supply-chain management and blockchain research. He is also a young and middle-aged leading talent in the field of cybersecurity and informatization of the Internet Information Office of the Jiangsu Provincial Party Committee, a talented person in innovation of Jiangsu Province, and a top expert in Nanjing. Previously, he was a senior researcher at IBM China Research Institute and a professor at the School of Management of Sun Yat-sen University. He is currently the Dean of Nanjing Trusted Blockchain and Algorithm Economics Institute, the chairman of Nanjing Jinninghui Technology, a visiting professor of Macau University of Science and Technology, a consultant on the Strategy Committee of Nanjing Digital Finance Industry Research Institute, and the chief scientist of the Blockchain Industry Finance laboratory of Foshan Rural Commercial Bank. He has presided over or participated in more than 10 National Natural Science Foundation projects and published more than 30 high-quality papers. He has 57 invention patents in the blockchain field and has obtained 53 software copyrights. He has served as a member of several academic committees, was named a highly cited scholar in China's decision science field by Elsevier for six consecutive years, and is one of the most influential scholars in China's decision science field.

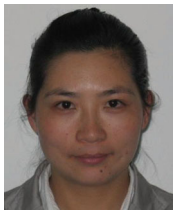

Tianjing Wang holds a BSc (2000) in Mathematics from Nanjing Normal University, an MSc (2005) in Mathematics from Nanjing University, and a PhD (2009) in Signal and Information System from Nanjing University of Posts and Telecommunications. From 2011 to 2013, she was a postdoctoral fellow with the School of Electronic Science and Engineering, Nanjing University of Posts and Telecommunications. From 2013 to 2014, she was a visiting scholar with the Department of Electrical and Computer Engineering, State University of New York at Stony Brook. She is now an Associate Professor in Mathematics at Nanjing Tech University. Her research interests include vehicular networks, UAV networking, and communications.

Guangwei Bai received the BEng and MEng degrees in computer engineering from Xi'an Jiaotong University, Xi'an, China, in 1983 and 1986, respectively, and the PhD degree in Computer Science from the University of Hamburg, Hamburg, Germany, in 1999. From 1999 to 2001, he worked at the German National Research Center for Information Technology, Germany, as a Research Scientist. In 2001, he joined the University of Calgary, Calgary, AB, Canada, as a Research Associate. Since 2005, he has been working at Nanjing Tech University, Nanjing, China, as a Professor in Computer Science. From October to December 2010, he was a Visiting Professor with the Department of Electrical and Computer Engineering, University of Waterloo, Waterloo, ON, Canada. His research interests include architecture and protocol design for communication networks, multimedia networking, network security, and location-based services. He is a member of the ACM and a Distinguished Member of CCF.

How to cite this article: Z. Tong, H. Shen, N. Shi, T. Wang, and G. Bai, *Joint resource optimization for nonorthogonal multiple access-enhanced scalable video coding multicast in unmanned aerial vehicle-assisted radio-access networks*, ETRI Journal **45** (2023), 874–886. https://doi.org/10.4218/etrij.2022-0136